Compressibility Effects in the Dynamics of the Reversed-Field Pinch

M. Onofri, F. Malara, and P. Veltri

Dipartimento di Fisica, Università della Calabria, ponte P. Bucci, Cubo 31C, 87036 Rende (CS), Italy

(Received 7 July 2008; published 18 December 2008)

We study the reversed-field pinch through the numerical solution of the compressible magnetohydrodynamic equations. Two cases are investigated: In the first case the pressure is derived from an adiabatic condition, and in the second case the pressure equation includes heating terms due to resistivity and viscosity. In the adiabatic case a single helicity state is observed, and the reversed-field pinch configuration is formed for short time intervals and is finally lost. In the nonadiabatic case the system reaches a multiple helicity state, and the reversal parameter remains negative for a longer time. The results show the importance of compressibility in determining the large scale dynamics of the system.

DOI: 10.1103/PhysRevLett.101.255002 PACS numbers: 52.65.Kj, 52.55.Hc

A reversed-field pinch (RFP) is a toroidal configuration, with minor radius a and major radius R, used to confine plasmas in fusion machines [1]. The poloidal (B_θ) and toroidal (B_ϕ) components of the magnetic field in a RFP are mostly generated by electric currents flowing in the plasma, and they are of the same order of magnitude. This configuration is characterized by a safety factor $q = rB_\phi/RB_\theta$ (r is the radial coordinate) which is less than unity in the core and negative at the edge, and the toroidal magnetic field changes sign at the edge with respect to the core. Because of this shape of the safety factor, many $m = 1$ and $n > R/a$ modes are resonant in the plasma, while the B_ϕ reversal surface is resonant for all $m = 0$ modes [1] (m and n are the poloidal and toroidal mode numbers, respectively).

Besides the interest in these kinds of machines as potential fusion reactors, they are also important for the study of fundamental issues like plasma relaxation, plasma turbulence, and its effects on plasma confinement. Many experimental studies have been addressed to the clarification of the mechanisms responsible for the formation and sustainment of the RFP configuration through a dynamo action induced by velocity and magnetic field fluctuations [2,3]. For many years, the plasma in RFP configurations has been observed in multiple helicity (MH) states characterized by several helicities m/n with comparable amplitudes in the magnetic spectrum. In recent years, different experiments [4,5] have shown the existence of quasihelical configurations. Single helicity (SH) or quasi-single helicity (QSH) states are believed to provide a better confinement with respect to turbulent RFP configurations. Experimental studies have shown the improvement in confinement associated with the presence of QSH states [6–8].

The RFP configuration has been also studied through numerical simulations of the magnetohydrodynamic (MHD) equations. Numerical simulations, based on a model with vanishing pressure and constant density [9,10], have shown that the RFP configuration can be sustained in a variety of regimes, which range from turbulent MH states to SH states [11,12]. In such a model, it has been noted that the existence of SH or MH states is controlled by the Hartmann number $H = (\mu\eta)^{-1/2}$ (μ and η are the dimensionless viscosity and resistivity, respectively) and pure SH states are observed in simulations for $H < 2000$ [12,13]. The magnetic field generated by these simulations has been used to study particle transport and plasma confinement [14].

In this Letter, we show that including compressibility in the simulations is not only a correction that modifies the details of the system behavior, but it also affects the large scale dynamics.

We describe the RFP plasma by a cylindrical geometry with coordinates (r, θ, z) such that $0 \le r \le 1$, $0 \le \theta \le 2\pi$, and $0 \le z \le 2\pi R$, and we solve the MHD equations in terms of the field variables density (ρ), momentum components $M_i = (\rho v_r, \rho v_\theta, \rho v_z)$, magnetic field components $B_i = (B_r, B_\theta, B_z)$, and thermal pressure p, in dimensionless form:

$$\frac{\partial \rho}{\partial t} = -\nabla \cdot \mathbf{M}, \tag{1}$$

$$\frac{\partial \mathbf{M}}{\partial t} = -\nabla \cdot \bar{\bar{F}} + \mathbf{J} \times \mathbf{B}, \tag{2}$$

$$\frac{\partial \mathbf{B}}{\partial t} = -\nabla \times \mathbf{E}, \tag{3}$$

$$\frac{\partial p}{\partial t} = -[\nabla \cdot (\mathbf{v}p - k_t \nabla T) + (\gamma - 1)p\nabla \cdot \mathbf{v}] + (\gamma - 1)H_p. \tag{4}$$

In Eq. (4), $\gamma = 5/3$ is the adiabatic index, T is the temperature $T = p/\rho$, and k_t is the thermal conductivity. In the simulations that we describe in this Letter, k_t has been set to zero assuming that typical values in RFP plasmas are very small, at least in the direction perpendicular to the magnetic field. The flux tensor $\bar{\bar{F}}$ in Eq. (2) has components

$$F_{ij} = M_i v_j + p\delta_{ij} - \mu\sigma_{ij}, \tag{5}$$

where σ_{ij} is the stress tensor. In the induction equation (3), the electric field $\mathbf{E}$ is given by the expression

$$\mathbf{E} = -\mathbf{v} \times \mathbf{B} + \eta \mathbf{J},$$

where $\mathbf{J} = \nabla \times \mathbf{B}$ defines the current density and η is the dimensionless resistivity. In the pressure equation (4), the heat production term H_p is given by

$$H_p = \eta J^2 + \mu[\tfrac{1}{2} U_{ij} U_{ij} - \tfrac{2}{3}(\nabla \cdot \mathbf{v})^2],$$

where the tensor U_{ij} is defined as

$$U_{ij} = \sigma_{ij} + \tfrac{2}{3}(\nabla \cdot \mathbf{v})\delta_{ij}. \quad (6)$$

We use the minor radius a of the torus (or the radius of the cylinder) as the unit length scale in the equations. We choose as the unit measure for the magnetic field and for the mass density typical values B_0 and ρ_0, respectively, which allows us to define a characteristic value for the Alfvén velocity $v_A = B_0/\sqrt{4\pi\rho_0}$. Hence, we normalize the velocity to v_A and the time to the typical Alfvén time: $\tau_A = a/v_A$. Finally, the pressure p is measured in units of $\rho_0 v_A^2$.

Boundary conditions at $r = 1$ are imposed assuming that the plasma is bounded by a conducting wall [15]. To obtain plasma relaxation with a field reversal, the system must be driven from the outside. This is realized assuming a constant toroidal current, which is equivalent to imposing a constant poloidal magnetic field at the boundary for the (0, 0) mode.

Space derivatives are computed using compact finite differences [16] along the radial direction r and with a pseudospectral method in the periodic directions. Time integration is given by a third-order Runge-Kutta explicit scheme.

As the initial state, a force-free equilibrium magnetic field has been chosen, characterized by the following safety factor [17]:

$$q(r) = q_0(1 - 1.8748r^2 + 0.832\,32r^4), \quad (7)$$

which is obtained by resistive diffusion from a stable configuration [18]. The dynamo action is demonstrated if the reversal of the axial field is maintained, which is controlled by the reversal parameter

$$F = \frac{B_z^{0,0}(a)}{\langle B_z \rangle},$$

where $\langle B_z \rangle$ is the average of the axial field over the poloidal cross section and $B_z^{0,0}(a)$ is the average of $B_z(a)$ in the θ and z directions.

Compressible MHD equations include heat production [last term of Eq. (4)] that, in contrast, plays no role in the incompressible case. One aim of the present work is to investigate the dynamical effect of heat production in the compressible case. One possibility is to neglect completely heat production. In this case, if the thermal conductivity is vanishing and if ρ and p are initially uniform, then Eq. (4) implies $p\rho^{-\gamma} = \text{const}$. Then, in the first simulation, we replace Eq. (4) by the adiabatic condition $p\rho^{-\gamma} = \text{const}$. On the contrary, in the second simulation, the full set of Eqs. (1)–(4) has been solved. Realistic values of the Reynolds numbers cannot be used in the numerical simulations due to the high resolution and computational time that would be necessary. Therefore, the Reynolds numbers used in the simulations are much smaller than the real ones, so that heat production occurs in the nonadiabatic simulation at spatial scales that are larger than in the real system. On the other hand, in the adiabatic simulation, heating is totally absent. The comparison between the adiabatic and the nonadiabatic runs can thus give us some insight about how the RFP dynamics is affected by the inclusion of heat production.

Both simulations have been carried out with $\eta = 2 \times 10^{-4}$, $\mu = 2 \times 10^{-4}$, and $k_t = 0$. Simulations with $q_0 = 0.4$ and an aspect ratio $R/a = 1$ have been performed in previous studies with uniform density and pressure [9,17]. An aspect ratio of 1 is unrealistic, but it has the advantage of requiring a lower resolution. With a larger aspect ratio, the dynamics of the system can change, since more modes are present. In Ref. [9], a simulation with an aspect ratio $R/a = 2$ and $q_0 = 0.2$ has also been described, and the results were in agreement with the case with $R/a = 1$ and $q_0 = 0.4$. In a previous work [15], we showed the importance of compressibility in simulations with $R/a = 1$ and $q_0 = 0.4$. The simulations described in the present Letter are performed with the more realistic values $R/a = 2$ and $q_0 = 0.2$.

The initial equilibrium is strongly unstable with respect to the $(m = 1, n = -4)$ mode [9]; therefore, the following perturbation has been superposed to the equilibrium field:

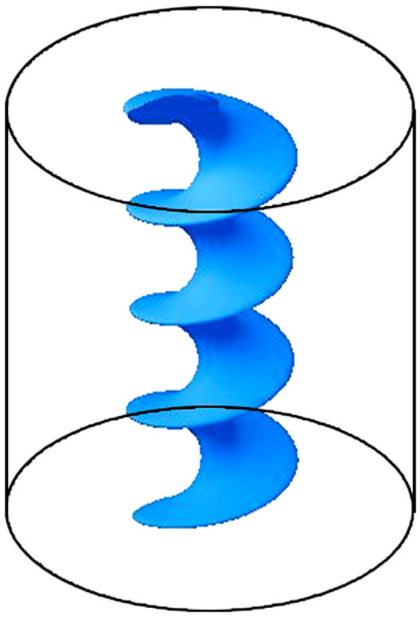

FIG. 1 (color online). Isosurface of the density in the adiabatic run at $t = 400$ and $\rho = 1.05$. The cylinder represents the whole spatial domain.

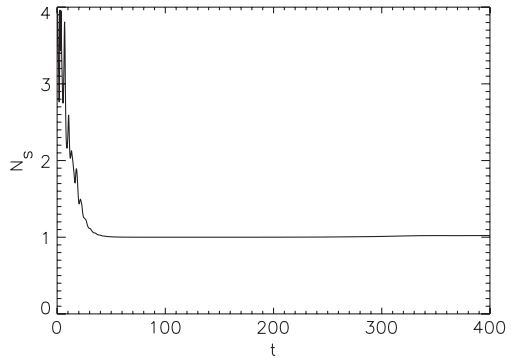

FIG. 2. The spectral spread N_s as a function of time in the adiabatic case.

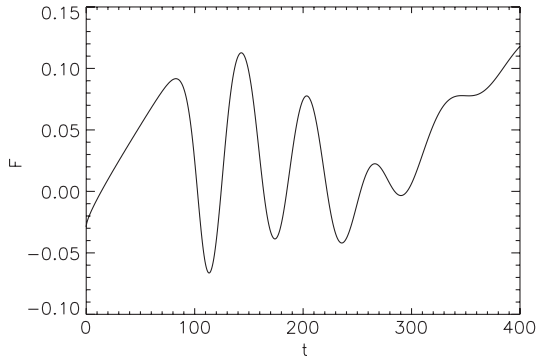

FIG. 3. Time evolution of the reversal parameter F for the adiabatic run.

$$v_r = \epsilon(1 - r^2) \sum_{n=-4}^{-1} \cos(\theta + nz/R), \tag{8}$$

$$v_\theta = \epsilon(1 - r^2) \sum_{n=-4}^{-1} \sin(\theta + nz/R). \tag{9}$$

The r dependence has been chosen to be compatible with the boundary conditions, and ϵ is the amplitude of the perturbation, which has been set to $\epsilon = 10^{-4}$.

The initial noise destabilizes the system, and the unstable modes begin to grow exponentially in the linear phase. In the first simulation (adiabatic case), after the formation of a SH state around $t = 30$, the system keeps this configuration until the end of the simulation at $t = 400$. The existence of a SH state is evident in Fig. 1, which shows the structure of the density at the end of the simulation. The density is concentrated near the axis of the cylinder, with the presence of a single dominant mode $m = 1$, $n = -4$. The states of single or multiple helicity can be identified by evaluating the spectral spread N_s [8], defined as

$$N_s^{-1} = \sum_n \left(\frac{B_{1,n}^2}{\sum_n B_{1,n}^2} \right)^2. \tag{10}$$

If $N_s \simeq 1$, the system is in a SH state; otherwise, it is in a MH state. The spectral spread N_s is shown in Fig. 2 as a function of time. In the first phase, many modes of comparable amplitudes are present due to the initial perturbations. After $t \simeq 50$, $N_s = 1$ and a SH state is maintained until the end of the simulation.

The time evolution of the reversal parameter F is shown in Fig. 3. After losing the reversal, the F parameter increases until $t \simeq 85$, then it shows an oscillatory behavior, becoming positive and negative several times, and, after $t \simeq 300$, F continues to increase until the end of the simulation.

The evolution of the system can be strongly modified by a weak heating caused by viscosity and resistivity. In the second run, we used Eq. (4) instead of the adiabatic condition. Differently from the adiabatic case, the system shows a transition from a SH state to a more turbulent MH state. The spectral spread N_s is shown in Fig. 4 as a function of time. After $t \simeq 50$, $N_s = 1$ and a SH state is maintained until $t \simeq 130$. At later times, N_s increases, and it reaches a maximum value above 3 at $t \simeq 190$, indicating a MH state. In Fig. 5, we show an isosurface of the density ρ for a MH state at $t = 190$. Contrary to what happens in the first run, the density is not only concentrated near the axis of the cylinder, there is a more complex structure, which is the result of the superposition of different helicities. As expected, plasma heating induces the growth of new modes at large scales. Even a relatively small value of the resistivity and viscosity produce enough heating to modify the mass distribution inside the cylinder, and the plasma is evacuated from heat production regions. The development of a broader energy spectrum implies the presence of smaller scales, which in turn makes the heating production even more effective.

The time evolution of the reversal parameter F is shown in Fig. 6. In the beginning of the simulation, the initial reversal is lost, and the reversal parameter F continues to increase until $t \simeq 50$. Later, the dynamo effect due to the growth of the instabilities makes F decrease and become negative again, reaching a minimum value $F \simeq -0.4$. Subsequently, it shows an oscillatory behavior, remaining below zero except for a short time around $t \simeq 90$. These

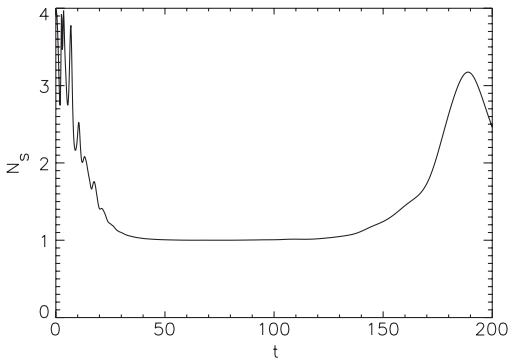

FIG. 4. The spectral spread N_s as a function of time in the nonadiabatic case.

FIG. 5 (color online). Isosurface of the density in the nonadiabatic run at $t = 190$ and $\rho = 1.2$, showing a MH state. The cylinder represents the whole spatial domain.

oscillations are not observed in simulations with constant density and vanishing pressure [10].

In both the adiabatic and the nonadiabatic cases, the behavior of the system is different from that derived for $p = 0$ and $\rho = \text{const}$. The effects of compressibility are not limited to secondary details, but the large scale dynamics of the system is affected, with consequences on fundamental aspects, like the persistence of the RFP configuration and the evolution of the reversal parameter.

By comparing the results obtained in the two simulations, we conclude that the system is very sensitive to the heating and the real RFP plasma probably exhibits an intermediate behavior between the two situations studied here. In the adiabatic case, we observe the formation of a SH state, with a small spectrum formed by the $m = 1$, $n = -4$ mode and its higher harmonics, but the RFP configuration is formed only for short time intervals and is finally lost. On the other hand, when the heating is present, we observe a transition from a SH state to a more turbulent MH state, with a larger spectrum. The excitation of small scales makes the heating even more effective, and its consequences on the system behavior become more important. The reversal parameter reaches more negative values, and it remains negative for a longer time.

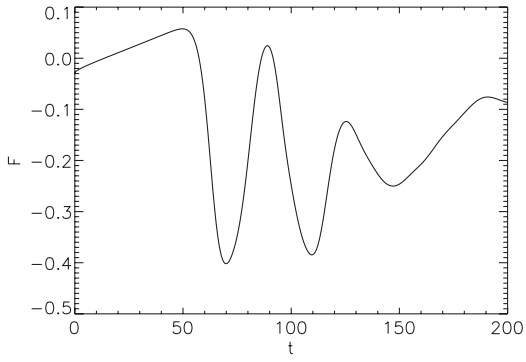

FIG. 6. Time evolution of the reversal parameter F for the nonadiabatic run.

These results suggest that compressible simulations are necessary for the numerical study of the dynamics of a RFP. On the other hand, including compressibility, it becomes clear that the model used to describe heat production is determinant to predict the behavior of the system. In the simulations described in this Letter, the Hartmann number is $H = 5000$ in both cases, which would give MH states in incompressible simulations. However, we find that the formation of SH or MH states and the evolution of the reversal parameter are controlled by the model used for heat production, which is not present in incompressible simulations. The results are different in the adiabatic and nonadiabatic cases, both of which are somewhat different from the real system. Including compressibility and using the correct model to describe heat production is therefore important to understand the dynamics of the RFP.

[1] P. Martin, Plasma Phys. Controlled Fusion **41**, A247 (1999).
[2] P. W. Fontana, D. J. Den Hartog, G. Fiksel, and S. C. Prager, Phys. Rev. Lett. **85**, 566 (2000).
[3] P. Piovesan, D. Craig, L. Marrelli, S. Cappello, and P. Martin, Phys. Rev. Lett. **93**, 235001 (2004).
[4] D. F. Escande, P. Martin, and S. Ortolani *et al.*, Phys. Rev. Lett. **85**, 1662 (2000).
[5] P. Martin, L. Marrelli, and G. Spizzo *et al.*, Nucl. Fusion **43**, 1855 (2003).
[6] D. Terranova, A. Alfier, F. Bonomo, P. Franz, P. Innocente, and R. Pasqualotto, Phys. Rev. Lett. **99**, 095001 (2007).
[7] M. D. Wyman, B. E. Chapman, and J. W. Ahn *et al.*, Phys. Plasmas **15**, 010701 (2008).
[8] L. Frassinetti, I. Predebon, H. Koguchi, Y. Yagi, Y. Hirano, H. Sakakita, G. Spizzo, and R. B. White, Phys. Rev. Lett. **97**, 175001 (2006).
[9] D. Merlin and D. Biskamp, Max-Planck-Institut für Plasmaphysik, Garching, Report No. IPP 6/276, 1988.
[10] S. Cappello and D. Biskamp, Nucl. Fusion **36**, 571 (1996).
[11] S. Cappello, Plasma Phys. Controlled Fusion **46**, B313 (2004).
[12] S. Cappello, D. Bonfiglio, and D. F. Escande, Phys. Plasmas **13**, 056102 (2006).
[13] S. Cappello and D. F. Escande, Phys. Rev. Lett. **85**, 3838 (2000).
[14] G. Spizzo, R. B. White, and S. Cappello, Phys. Plasmas **14**, 102310 (2007).
[15] M. Onofri, L. Primavera, F. Malara, and P. Londrillo, J. Comput. Phys. **226**, 1874 (2007).
[16] S. K. Lele, J. Comput. Phys. **103**, 16 (1992).
[17] D. D. Schnack, D. C. Barnes, Z. Mikic, D. S. Harned, and E. J. Camarana, J. Comput. Phys. **70**, 330 (1987).
[18] D. C. Robinson, Nucl. Fusion **18**, 939 (1978).